Prominence Seismology: Wavelet Analysis of Filament Oscillations

Pintér, Balázs; Jain, Rekha; Tripathi, Durgesh; Isobe, Hiroaki

Published in:
Astrophysical Journal

DOI:
10.1086/588273

Publication date:
2008

Citation for published version (APA):
Pintér, B., Jain, R., Tripathi, D., & Isobe, H. (2008). Prominence Seismology: Wavelet Analysis of Filament Oscillations. *Astrophysical Journal*, *680*, 1560-1568. https://doi.org/10.1086/588273

The Astrophysical Journal, 680:1560–1568, 2008 June 20

PROMINENCE SEISMOLOGY: WAVELET ANALYSIS OF FILAMENT OSCILLATIONS

Balázs Pintér
Institute of Mathematics and Physics, Aberystwyth University, Penglais Campus, Physics Building, Aberystwyth SY23 3BZ, UK
Rekha Jain
Department of Applied Mathematics, University of Sheffield, Sheffield S3 7RH, UK
Durgesh Tripathi
Department of Applied Mathematics and Theoretical Physics, University of Cambridge, Cambridge CB2 1ND, UK
and
Hiroaki Isobe
Department of Earth and Planetary Science, University of Tokyo, Tokyo 113-0033, Japan
Received 2007 September 10; accepted 2008 March 15

ABSTRACT

The temporal and spatial behavior of a large-amplitude filament oscillation is investigated using wavelet analysis. The extreme-ultraviolet (EUV) images of the phenomenon, which occurred on 2002 October 15, were taken from the EUV Imaging Telescope on board the *Solar and Heliospheric Observatory* (*SOHO*). The wavelet spectra, extracted from the intensity data, show that the filament oscillates as a rigid body, with a period of about 2.5–2.6 hr which is almost constant along the filament. The period slowly decreases with time until the filament erupts. No clear sign of the eruption is found in the wavelet spectrum prior to the eruption, that followed the filament oscillation. The axial component of the magnetic field is estimated between 1 and 5 G, which is believed to be reasonable for a polar crown filament of this kind.

Subject headings: Sun: activity — Sun: corona — Sun: filaments — Sun: oscillations

Online material: color figures, mpeg animation

1. INTRODUCTION

It has been known for more than half a century that the solar filaments exhibit large-amplitude oscillatory motions induced by some solar disturbances such as solar flares. Large-amplitude oscillations of prominences often referred to as the "winking" filaments (see, for example, Ramsey & Smith 1966), believed to be triggered by remote flares, are observed on the solar disk. Recently, with the help of better quality observations from the ground- and space-based instruments, the triggering disturbances in many filaments have been identified as Moreton (Moreton 1960) and/or EUV Imaging Telescope (EIT) waves (Thompson et al. 1999). Large-amplitude oscillations can occur either perpendicular to the filament axis (see, e.g., Eto et al. 2002; Okamoto et al. 2004) or along the axis (see, e.g., Jing et al. 2003, 2006; Vršnak et al. 2007).

Theoretical studies to understand the periodicities, amplitudes, and the damping mechanisms are carried out in the framework of magnetohydrodynamics (MHD; see, e.g., Kippenhahn & Schlüter 1957; Kleczek & Kuperus 1969; Oliver et al. 1992; Vršnak 1993; Roberts 2000; Díaz et al. 2001; Ruderman & Roberts 2002; Oliver & Ballester 2002; Ballai 2003; Terradas et al. 2005). Combining observations and theory of prominence oscillation is emerging as an exciting tool for probing magnetic field structure and other plasma properties, giving rise to the new field of *prominence seismology* analogous (as a diagnostic tool) to the well-known field of helioseismology.

Despite there being a period of more than 50 years since the first observational reports on the prominence oscillations and recent advancements in both theoretical and observational efforts to identify them, it remains a puzzle as to: What triggers the large-amplitude oscillations of filaments in the absence of a flare? What is the nature of these oscillations? Are these oscillations standing modes or propagating? What slows down that which, in principle, should be the most energetic oscillatory phenomenon in the solar corona? What causes the prominence eruptions?

In this paper, we present a clear, scientific investigation of the large-amplitude oscillatory phenomenon of a filament reported by Isobe & Tripathi (2006, hereafter IT06; see also Isobe et al. 2007). IT06 reported that the oscillatory motion of the polar crown filament that erupted on 2002 October 15 was predominantly horizontal, and the line-of-sight velocity was estimated to be about few tens of km s^{-1} (see also Isobe et al. 2007). IT06 visually estimated the period of oscillation to be 2 hr and, based on the model by Kleczek & Kuperus (1969), estimated the Alfvén velocity to be 12 km s^{-1}. Here, we carry out the wavelet analysis to find the period more accurately and to study the temporal and spatial behavior of the oscillating filament. The paper is organized as follows. In § 2 we describe the observations and methods used for data analysis. The results are discussed in § 3, followed by conclusions in § 4.

2. OBSERVATIONS AND ANALYSIS METHOD

The filament oscillation that we discuss in this paper was seen on 2002 October 15 at about 02:50 UT and completed three cycles before erupting. The EUV images were taken by the EIT (Delaboudiniere et al. 1995) on board the *Solar Helioseismic Observatory* (*SOHO*) satellite (Domingo et al. 1995). The EIT provides full-disk images of the Sun at 195 Å among others with the regular cadence of 12 minutes. The emission in the 195 Å passband of the EIT is dominated by an Fe XII line forming at 1.5 MK, but also contains Fe XXIV line forming at 20 MK, which is much weaker in the quiet-Sun region but highly significant in the flaring region (Tripathi et al. 2006a, 2006b). The online version of the article is accompanied by two animated files, which show the

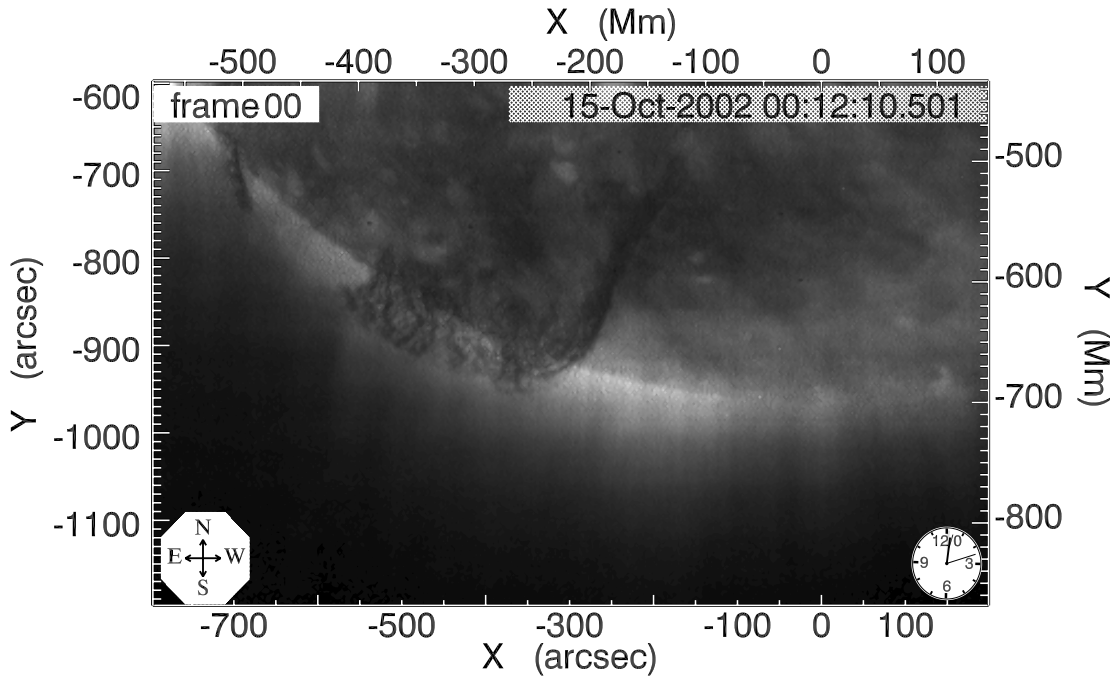

FIG. 1.— *SOHO* EIT image taken at 195 Å showing the oscillating prominence on 2002 October 15. The prominence at the southern limb of the solar disk appears dark due to a decrease in intensity. The position coordinates, *X* and *Y*, are given in arcseconds and megameters. [*See the electronic edition of the Journal for a color version and mpeg animation of this figure.*]

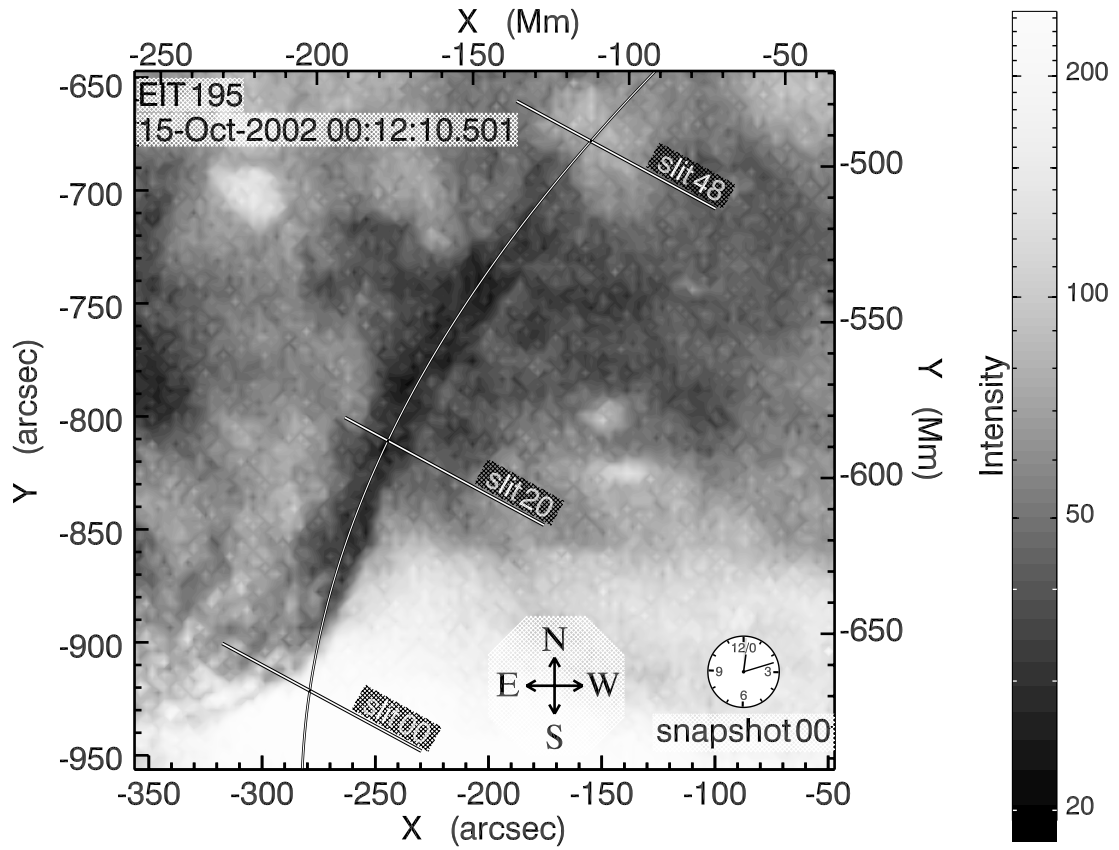

FIG. 2.— EIT image of the filament prior to its oscillation. The white curve is a parabola fitted to the filament. The straight lines are three of the 49 equally spaced, parallel slits, along which the temporal variation of the intensity distribution is studied. This region (without the white curves) is a part of Fig. 1. [*See the electronic edition of the Journal for a color version and mpeg animation of this figure.*]

motion of the filament. Figures 1 and 2 are the first snapshots of the two animations. A huge prominence takes place in the southeast (bottom left) "corner" of the solar disk, near the southern pole of the Sun. The prominence appears in the intensity map as a dark, slightly elongated and tilted "U" shape. The footpoints (the two upper points of the U shape) appear about 600″ (430 Mm) distance apart. The first online movie (with its first snapshot given in Fig. 1) shows the motion of the entire prominence. The animation is made of 64 EIT images of 2.6″ spatial and 12 minute temporal resolution. The frame ranges horizontally between −800″ and 200″, and vertically between −1200″ and −600″. The large and thick top of the prominence is rising slowly until it is blown away as a huge eruption (see IT06).

The right foot of the prominence is a long filament, which runs from bottom left, at about (−300″, −900″), to top right, at about (−130″, −500″), at the beginning. This filament shows an oscillatory motion, lasting for several periods. The subject of this analysis is the oscillation of this filament. This part of the prominence is enlarged in the second movie. The first snapshot can be seen in Figure 2. The frame ranges horizontally between −360 and −50″, and vertically between −960″ and −650″.

The region shown in Figure 2 is the only part of the prominence that exhibited the oscillation, although the whole prominence eventually erupted after the oscillation (see IT06). The first image, in Figure 2, was recorded at 00:12:10.501 UT. The filament can be identified as a dark curve, overarching the frame from bottom to top. The darkness of the prominence indicates a fall of intensity along the curve due to a lower temperature than the surrounding plasma. The oscillatory motions started at about 02:50 UT, and on the basis of the velocity field IT06 noted that the oscillations were perpendicular to the filament axis and that the filament probably belonged to the winking filament type due to their appearance and disappearance, in blue and red wings of Hα, respectively, on the plane of sky.

The online movie of the observed filament (with the first snapshot in Fig. 2) clearly shows that it is drifted toward west due to solar rotation.

The three parallel straight lines labeled as slit 0, slit 20, and slit 48 in Figure 2 are three slits, along which the filament motion is followed. Slit 0 is the lowest, while slit 48 is the uppermost slit. The coordinates of the two ends of slit 0 in arcseconds are (−318″, −900″) and (−230″, −948″), and for slit 48 are (−188″, −660″) and (−100″, −708″). There are 47 additional slits (slits 01–47) considered between the lowest and uppermost ones. They are equally distributed, parallel to each other, and have the same length. Displaying all the slits would hide the filament itself, and hence, only slit 00 (the lowest), slit 20 (corresponding to the inner part of the filament), and slit 48 (the uppermost) are shown in Figure 2. Slit 20 will be used later as an example for illustration. The length of each slit is 100″. The slits are not shown in the online animations. The position and the size of the slits were chosen to cover the area swept by the filament during its existence.

The next important step in the analysis is to find the position of the filament along each slit on each of the 62 intensity maps. One way to achieve this is to fit a quadratic polynomial (a parabola) to the two-dimensional intensity distribution of the filament region. The intersection of the parabola with a slit is considered as the position of the filament on the given slit. The position is given by the distance of the intersect measured from the upper left endpoint of the slit. We will refer to this method of position finding as the "global fitting" method. The parabola fitted to the filament in the first image is shown in Figure 2. This method considers the filament basically as one compact object.

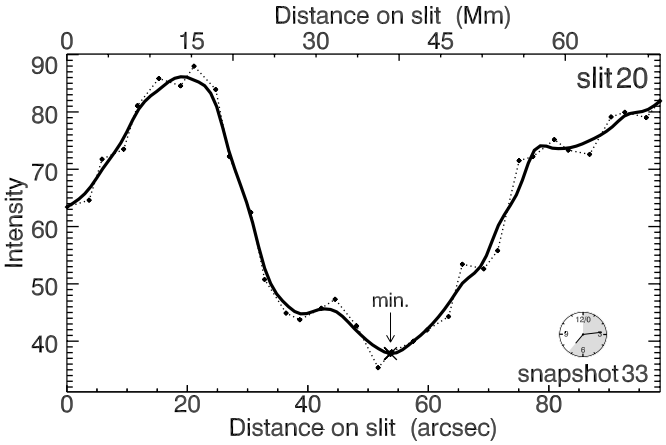

FIG. 3.—Intensity distribution along slit 20 for snapshot 33. The intensity "pit" is showing the cross section of the filament along the slit. The distance from the upper left endpoint of the slit (see its position displayed in Fig. 1) is given on the horizontal axes in arcseconds and megameters. The actual intensity values read from the EIT data are plotted with the dotted line; the solid line is its smoothed version. The minimum position of the smoothed intensity distribution ("min.") is considered the actual reference position of the filament at this slit. [*See the electronic edition of the Journal for a color version of this figure.*]

A more detailed view of the filament motion can be obtained by a second way of identifying the filament position along the slits. We consider each slit and find the intensity distribution along the slit from each of the 62 snapshots. This intensity distribution is shown for slit 20 and snapshot 33 (07:13:48.646 UT) in Figure 3 by the dotted line. The distance from the upper left endpoint of the slit is given in arcseconds and megameters. The resulting curve is then smoothed out by replacing each value by the running mean, taking into account the intensity values at the neighboring points along the slit. Finally, the solid curve is obtained by interpolation in order to increase the sampling along the slit. The cross section of the filament cut by the slit appears as an intensity pit. The position of the local minimum (the bottom of the pit, labeled "min." in Fig. 3) now represents the filament position. We will refer to this method as the "minimum search" method.

We also tested a third way to determine the position of the filament along a slit by fitting an upside-down Gaussian to the pit and considering the minimum place of the fitted curve to be the filament position. However, a fully automatized fitting procedure was not possible due to the scattered intensity distribution along most of the slits, and the Gaussian extremes diverged significantly from the expected filament position. Thus, rather than carrying out the Gaussian fitting for each slit at each time, we restrict ourselves to the two methods described above to be more reliable.

3. RESULTS AND DISCUSSION

Figure 4 is a summary diagram of the two methods of position finding, which are described in the previous section, for slit 20 as an example. The time of the snapshots runs along the horizontal axis. The vertical axis represents the distance from the upper left endpoint of slit 20, given in arcseconds and megameters. The intensity distribution along slit 20 is given by a color bar for each of the 62 snapshots. The width of each bar equals the cadence, 0.2 hr. The two gaps, at 1 and 7 hr, are due to gaps in the EIT data at those times. The darker regions within a snapshot represent lower intensity. Regions with intensity larger than 40% of the maximum intensity for the given snapshot are kept white to show the motion of the intensity pit clearly. The darkest part at each snapshot is identified as the filament position on the slit

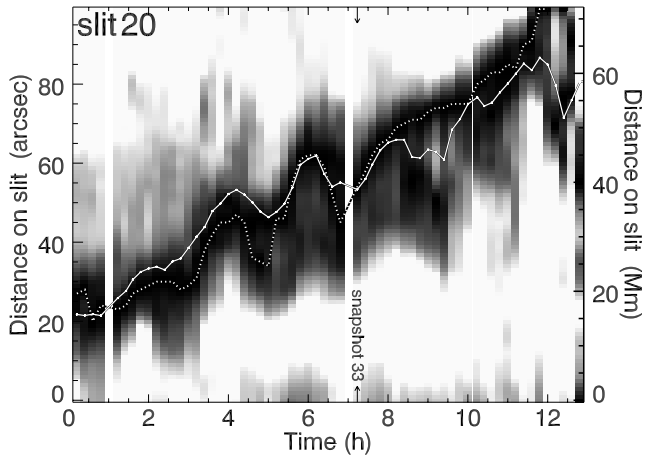

FIG. 4.—Intensity distributions along slit 20 for snapshots 0–61. The solid and dotted lines indicate the filament position determined by the global fitting and minimum search methods, respectively. [*See the electronic edition of the Journal for a color version of this figure.*]

according to the minimum search method. These points are joined by the dotted line. The filament positions obtained by the global fitting method are plotted with a solid line. This figure shows the global character of this method, as the positions do not necessarily take place at the bottom of the pits; however, they are still somewhere within the pit, and they clearly show the oscillatory motion of the filament. It can be seen that the intensity distribution displayed in Figure 3 matches well with the snapshot 33 (labeled), at $t = 07:13:48.646$ UT of Figure 4. The example, slit 20, used in Figure 4 to display the oscillation, is deliberately chosen from the middle part of the filament, as the oscillatory motion gradually vanishes toward the two endpoints of the filament. It is also apparent in Figure 4 (see also the online movies) that the filament, besides oscillating, is shifted to the right along the slits. (Recall that the distance of the filament on each slit is measured from its left end; therefore, an upward shift in Fig. 4 is equivalent to a right shift along a slit, e.g., in Fig. 3.) The right shift is most likely due to the slow rise of the prominence during the oscillation (see movie 1 online).

The speed of the filament shift at slit 20 is about 5 arcsec hr^{-1} (or about 1 km s^{-1}). We remove this constant motion from the distance versus time (by linear fitting of the data) to study the oscillatory motion. The resulting velocity oscillation along slit 20 is plotted in Figure 5 as obtained from the minimum search (*dashed line*) and global fitting (*solid line*) methods. The velocity amplitude of the oscillation increases from about 15 arcsec hr^{-1} (3 km s^{-1}) to about 35 arcsec hr^{-1} (7 km s^{-1}) during two or three oscillation periods, then it starts to decrease.

The dots joined by the solid line show the temporal variation of the filament position on slit 20, as an example, after the linear trend (a slow rise motion, which appears as a right shift) is removed from the data, which were obtained by the global fitting method. The oscillatory motion of the filament position along slits 10, 15, 20, 25, and 30 can be seen in Figure 6. The dots joined by a thin solid line show the temporal variation of the filament position on each of the five selected slits, after the linear trend (due to a rise motion) is removed from the data, which were obtained by the global fitting method. The resulting curve is then smoothed out (*thick line*) by replacing each value by the running mean, taking into account the intensity values at the neighboring points (in the same way as was done in Fig. 3). Finally, the solid curve is obtained by interpolation in order to increase the sampling along the slit (in the same way again as in Fig. 3). It can be seen that the filament position oscillates basically in phase along the slits. The amplitudes of oscillation seem to increase with increasing slit number (as moving along the filament toward the right footpoint of the prominence).

To investigate the temporal behavior of the oscillation, we wavelet analyze the position versus time data series. Wavelet analysis is a powerful technique to investigate the temporal variation of oscillations occurring in a dynamic system. We use the Morlet wavelet as mother wavelet with wavelet parameter value of 6 throughout the wavelet analysis. Figure 7 shows three wavelet spectra of the filament motion along slits 15, 20, and 25 (see Fig. 6). The wavelet spectra are displayed as an intensity map of the oscillation period (or also frequency) as a function of time. The analysis is reliable for the intermediate time intervals. The two sides of the unreliable part (so-called cone of influence) of the spectrum are shaded in Figure 7. The strongest periods of the spectrum are marked by a dot. The straight line is the best linear fit to the strongest periods. Each wavelet spectrum clearly shows that the dominant oscillation period is about 2.5 hr (0.11 mHz frequency),

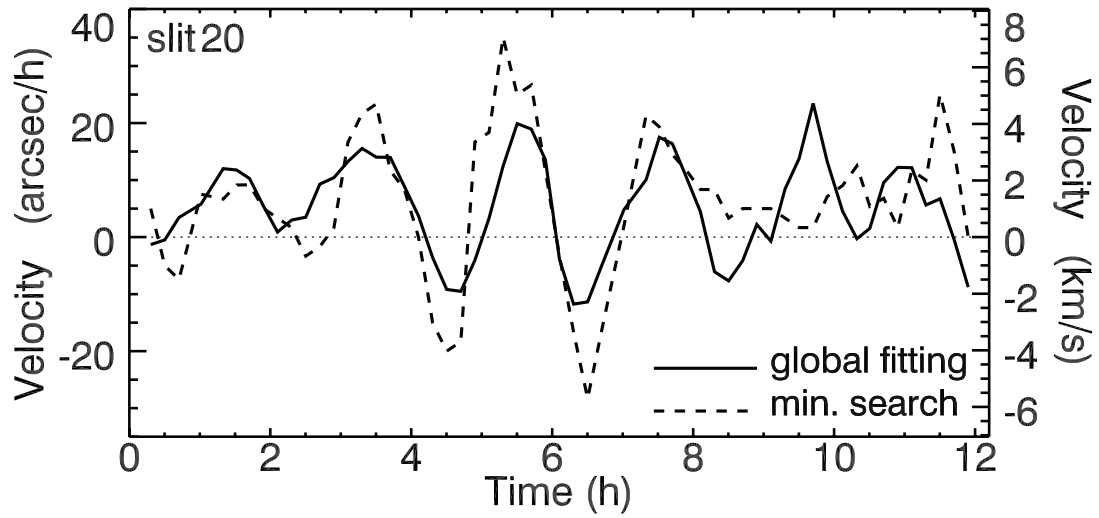

FIG. 5.—Speed of the motion of the filament position along slit 20 as a function of time. The filament positions are displayed in Fig. 4. The velocity data determined by both the global fitting method (*solid line*) and the minimum search method (*dashed line*) clearly show four complete oscillations. The velocities are given in arcsec hr^{-1} and km s^{-1} on the vertical axes. [*See the electronic edition of the Journal for a color version of this figure.*]

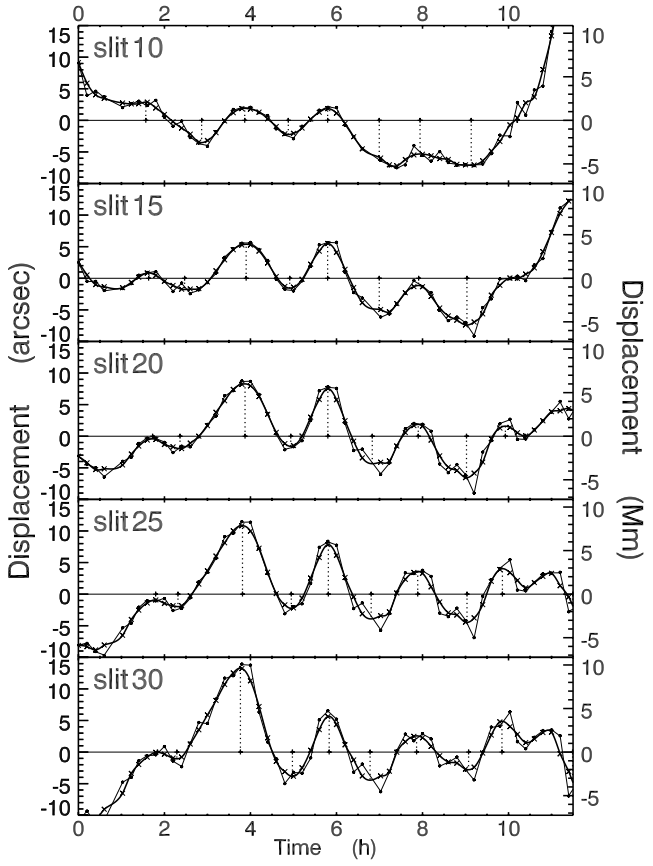

FIG. 6.— Filament positions (in arcseconds and megameters) determined by the global fitting method on slits 10, 15, 20, 25, and 30. The linear trend and the mean distance on the slit are removed. [*See the electronic edition of the Journal for a color version of this figure.*]

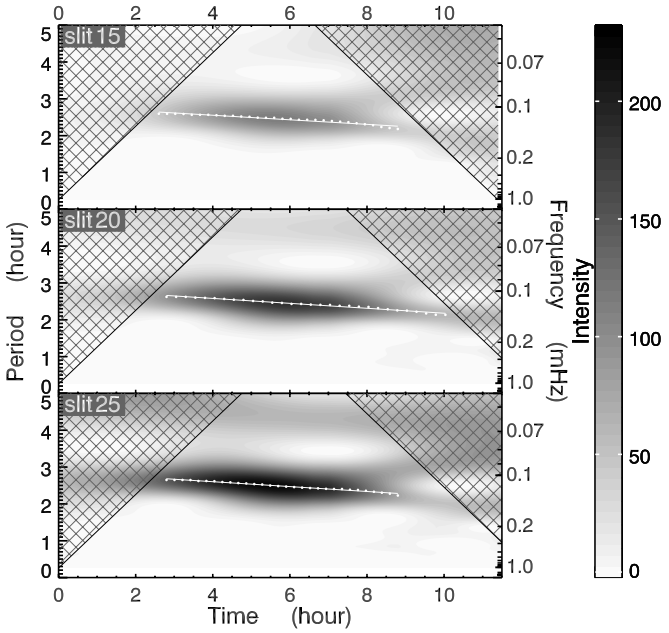

FIG. 7.— Wavelet spectrum of the filament position determined by the global fitting method. The average of the dominant periods for every snapshot, marked by dots, gives the dominant oscillation period for each slit. The solid line is the linear trend of the dominant periods. [*See the electronic edition of the Journal for a color version of this figure.*]

and it slowly decreases with time, dropping from 2.6 hr (0.1 mHz) to 2.1 hr (0.13 mHz) in 7 hr.

This analysis is done for the filament motion along each of the 49 slits. The results are displayed in Figures 8–11. Although the oscillation cannot be seen clearly near the two endpoints of the filament, the graphs are extended to the whole range of slits. The oscillatory behavior is evident between slits 12 and 37.

Oscillations cannot be seen either by an eye inspection of the animated images of the intensity maps or in the wavelet spectrum for the two sections covering slits 0–6 and slits 42–49. The filament movement in these regions, which may resemble fluctuations, turns out to be rather stochastic, noisy motion when analyzing the temporal variation of the filament position along the individual slits. These two regions are shaded dark in Figures 8–11. The intermediate or transitional regions, for which the wavelet analysis does not provide clear evidence of oscillation for a significant time span, are shaded with a lighter tone. The mean and the changing rate of the dominant periods in the shaded regions are therefore not considered to be real oscillations. We infer from this analysis that the largest amplitude of oscillation was in the middle part of the filament, with negligible motions at the filament ends suggesting a standing mode oscillation analogous to a slinky which is fixed at both ends.

Figures 8 and 9 show the average of the dominant periods obtained for each slit from the wavelet spectra of the data derived by the global fitting method (Fig. 8) and by the minimum search method (Fig. 9) as a function of slits. The error bars on the graphs are small, as they are obtained from the standard deviation of the dominant periods at each time. Hence the error bars simply show how large the change of rate of the oscillation period at a given slit is. The dominant periods and their decrease at slits 15, 20, and 25 can be seen in Figure 7, where the dominant period decreases. The average of the dominant periods over the slits obtained from the global fitting method (Fig. 8) is 2.532 ± 0.004 hr, which is close to the range obtained from the minimum search method, 2.6 ± 0.01 hr. The oscillation period seems to decrease slightly toward the center of the filament in Figure 8. The change is less than 20%, which is within 1 standard deviation of the overall data. However, this small but systematic change is not evident in Figure 9, which is obtained by using the minimum search method.

It should be noted that in the minimum search method, the result for one slit does not depend on the filament position of the surrounding slits, unlike in the global fitting method (shown in Fig. 8). We can conclude from these results that, although the filament does not oscillate as a solid object, its period does not vary significantly from its one end to the other, at least in the part where our analysis is reliable, i.e., in the unshaded part of Figures 8 and 9.

The temporal development of the oscillation period of the filament section of each slit is investigated by fitting a linear trend to the dominant periods shown by the wavelet spectra. The linear trends for slits 15, 20, and 25 are shown in Figure 7, while the average of the dominant periods is shown in Figures 8 and 9. The slopes of the resulting 49 trend lines, which are the mean changing rates of the dominant oscillation period at each slit, are shown in Figures 10 and 11 for the methods of global fitting and minimum search, respectively. Although the values are more scattered in Figure 11 than in Figure 10, both are dominantly in the negative domain. The mean of the changing rates of the dominant periods (for slits between 12 and 37, where the filament oscillation is clearly seen) from the global fitting method (Fig. 10) is -0.035 ± 0.006, while that obtained from the minimum search method (Fig. 11) is -0.061 ± 0.018. (Note that the changing rates of the dominant periods are dimensionless, as they are derivatives of a timelike quantity with respect to time.) Thus,

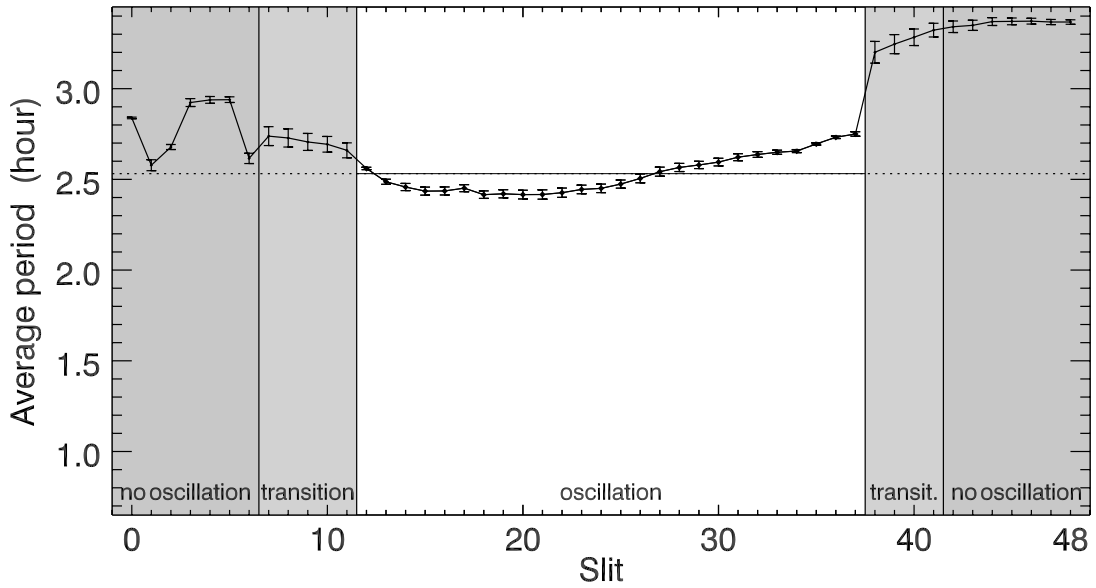

FIG. 8.—Average of the dominant oscillation periods for each slit (see Fig. 7 for slits 15, 20, and 25) as obtained by the global fitting method. [*See the electronic edition of the Journal for a color version of this figure.*]

the average period of oscillation decreases slowly with time. The physical origin of this decrease of the average period is not clear.

In order to further investigate whether the oscillations are propagating or standing, we study in detail the time when oscillation peaks occur in each slit. Recall that the peaks are clearly seen between slits 12 and 37, and not recognizable between slits 0 and 6, and between slits 42 and 49. We can identify five positive and five negative peaks by finding local minimum and maximum places in the filament position versus time graphs obtained from the global fitting method, and four positive and four negative peaks in the graphs obtained from the minimum search method. For example, the time when the five positive and five negative peaks occurred on slits 10, 15, 20, 25, and 30 are marked in Figure 6 by plus signs (joined by dotted lines) along the horizontal axis. Note that a time for a positive peak means that the filament reaches its maximum distance to the right at that time in the given slit, while a time for a negative peak means that the filament reaches its maximum distance to the left at that time in the given slit.

These identified "peak times" taken from all the 49 slits are shown in Figures 12 for the global fitting and minimum search methods, respectively, and in Figure 13, where each dot represents a peak occurring on a slit at a certain time. The horizontal axis shows the time when the peak occurred, while the slit where the peak time is measured and the distance of the slit (measured from slit 0 in megameters) is given on the vertical axes. This indicates that the points which represent peaks occurred in the *same slit* appear at the *same height* in Figures 12 and 13. For example, the uppermost four points in Figure 12, representing peaks at the early time of the oscillations, are plotted at 198 Mm, as they belong to slit 48, for which the distance from slit 0 is 198 Mm. In the cases when the peaks are not clearly identifiable, the peaks

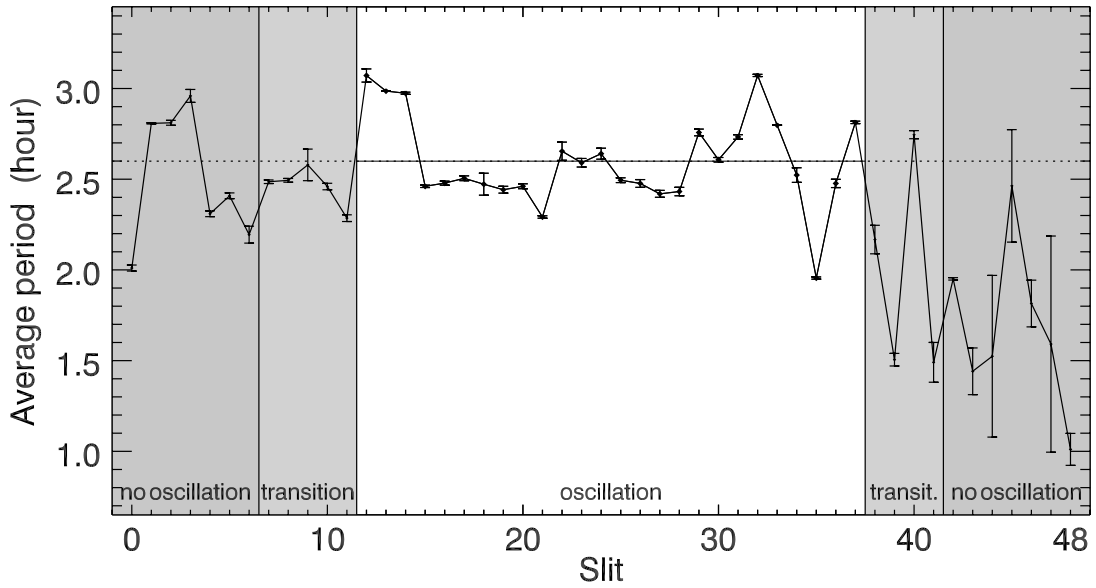

FIG. 9.—Average of the dominant oscillation periods for each slit as obtained by the minimum search method. [*See the electronic edition of the Journal for a color version of this figure.*]

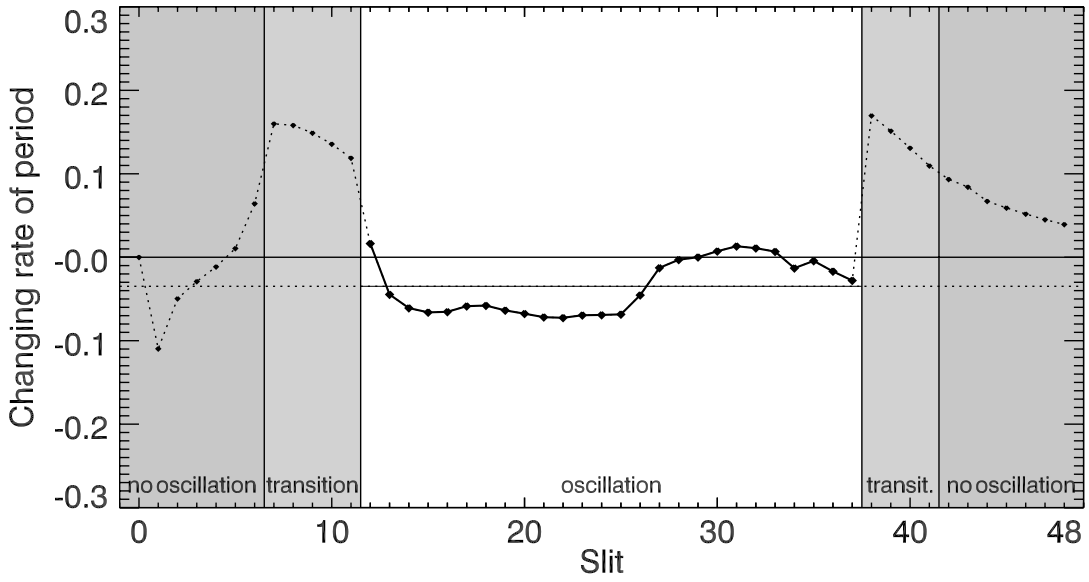

FIG. 10.— Rate of change of the dominant oscillation periods for each slit by using the global fitting method. The rate of change is obtained by measuring the slope of the linear trend line of the dominant periods (see the trend lines in Fig. 7). [*See the electronic edition of the Journal for a color version of this figure.*]

are not shown. The dots belonging to the same peak are joined by a solid line.

The time when a peak actually occurred can be obtained from the graph by reading the horizontal coordinate. The slope of the linear trend of each graph provides an estimate of how fast the peak phase propagates along the filament (from slit to slit), which is a way to estimate a phase speed of longitudinal propagation. The graphs are almost vertical due to the fact that the differences in the time when a certain peak occurs in different slits are much smaller than the characteristic period of the (transverse) oscillation of the filament. For a qualitative study, we can fit a linear trend line to the graphs, taking into account those points only, which are taken from the slits, where the oscillation is clearly seen, that is, from slits 12 to 37 (at a distance from slit 0 between 49.5 and 152.6 Mm). The slope of the 10 graphs in Figure 12 is $v_{\rm phase} = (-176.7 \pm 193.5)\,{\rm km\,s^{-1}}$. The slope of the eight graphs in Figure 13 is $v_{\rm phase} = (-0.4 \pm 5.3)$ km s^{-1}. The error bars, obtained from both methods, are larger than the average slopes. From this we can conclude that there is no *global* wave propagation *along* the filament, $v_{\rm phase} \approx 0$, but the *global* oscillation is transverse. We cannot completely rule out that some internal structure in the filament may be responsible for this small phase velocity (there is some evidence of few blobs oscillating along the filament; please see the attached movies of Figs. 1 and 2). We can confidently say that at least the *global* oscillation is a standing mode (possibly with a small contribution from the internal motion of the filament).

The filament oscillation seems to have been triggered due to magnetic reconnection between a nearby emerging magnetic flux and a filament barb (see also Isobe et al. 2007). However, the energy release was probably too small to show flarelike brightenings in Hα and EIT images just before the oscillation started. Eruption of prominences have been studied observationally as

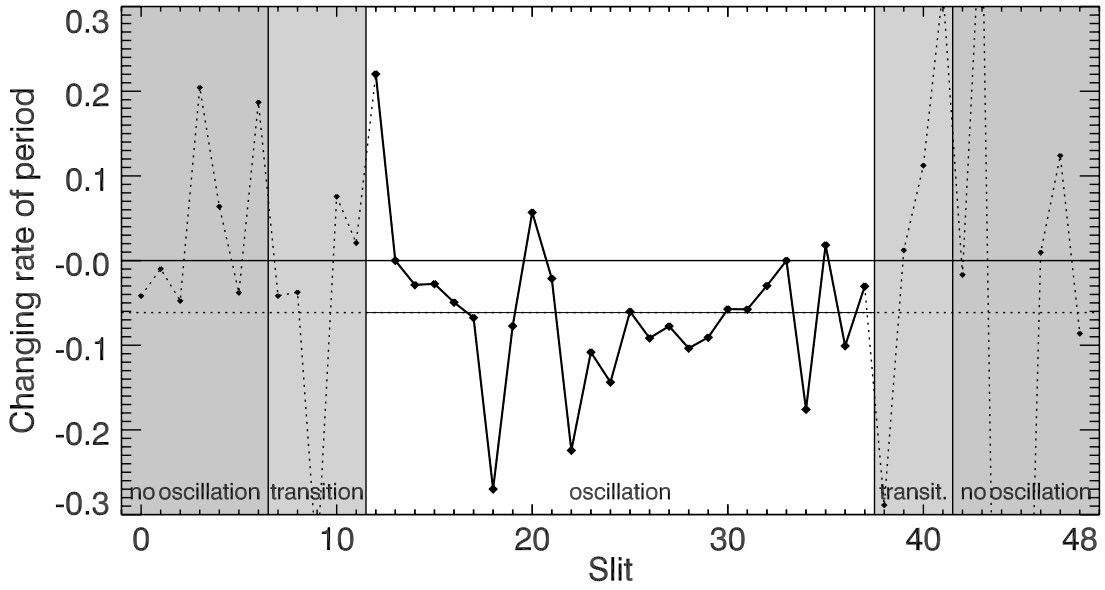

FIG. 11.— Slope of the dominant oscillation periods for each slit as obtained by the minimum search method. [*See the electronic edition of the Journal for a color version of this figure.*]

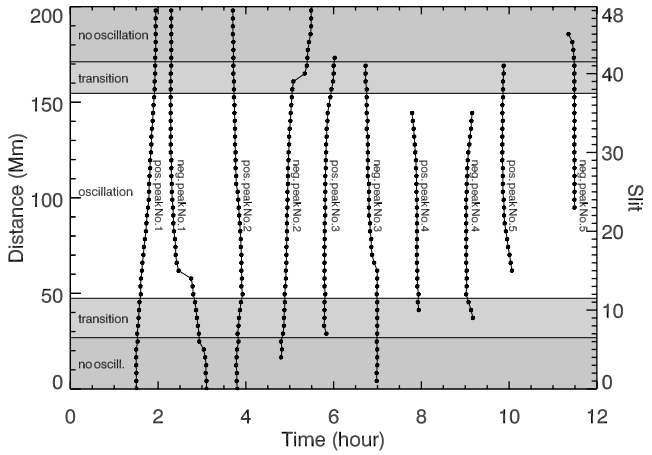

FIG. 12.—Distance of the slits in megameters, measured from slit 0, as a function of the time when a peak occurred during the oscillatory motion of the filament at the given slit. The filament position on the slit is determined by the global fitting method. [*See the electronic edition of the Journal for a color version of this figure.*]

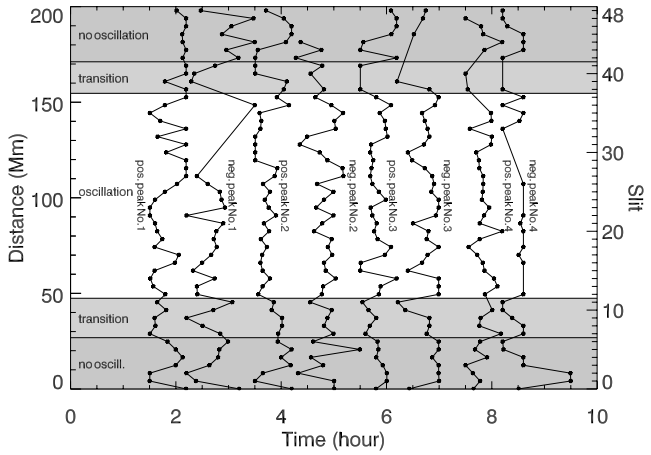

FIG. 13.—Distance of slits in megameters, measured from slit 0, as a function of the time when a peak occurred during the oscillatory motion of the filament at the given slit. The filament position on the slit is determined by the minimum search method. [*See the electronic edition of the Journal for a color version of this figure.*]

well as theoretically (e.g., Bruzek 1952; Feynman & Martin 1995; Wang & Sheeley 1999; Chen & Shibata 2000; Lin et al. 2001; Tripathi 2005; Chifor et al. 2006; Ballester 2006). Bearing in mind that this is a polar crown filament, the magnetic field strength is not likely to be very strong.

Following Vršnak (1990; see also Vršnak et al. 1991), we can assume a scenario where the filament is a twisted flux ropelike structure of a uniform cross section with both ends fixed. Unfortunately, the pitch angle of the filament was not measured before or after the eruption, but it is possible that even after the filament was activated by the magnetic reconnection, the filament evolved for the next few hours in such a way that the initial "twist" distribution along the axis of the filament did not change much. We can call this phase relatively stable. During the oscillation, some internal three-dimensional resistive instability and/or slight mass loss may have "detwisted" the initial twist, leading to sudden eruption of the filament. Based on this scenario, we can estimate the poloidal and axial components of the magnetic field strength, following Vršnak et al. (2007), by assuming that a certain amount of poloidal flux, as a result of magnetic reconnection, was injected into the filament. Considering the number density of the equilibrium plasma to be 10^{10}–10^{11} cm^{-3} in the filament, and the Alfvén speed, $v_{A\phi}$, corresponding to the equilibrium poloidal field $B_{\phi 0}$ as

$$v_{A\phi} = \frac{\sqrt{2}\pi L}{P} \approx 49 \text{ km s}^{-1},$$

where $2L = 200$ Mm is the length of the oscillating filament and P (=2.5 hr) is the average period (see Figs. 8 and 9), we obtain $B_{\phi 0} \approx 2$–10 G. Since the exact value for the pitch angle is not known, it is difficult to obtain the axial magnetic field strength in the stable phase of the prominence. Estimating the mean value of pitch angle as $\theta = 65^\circ$ and considering $\tan\theta = B_{\phi 0}/B_\parallel$, where $B_\parallel$ is the axial component of the magnetic field, we find $B_\parallel \approx 1$–5 G, which is reasonable, as this is a polar crown filament, and so we expect it to have a weak magnetic field.

Note that the oscillation period from the wavelet analysis is estimated to be 2.5 hr, which is different compared to IT06, who quoted 2 hr. This difference is due to the fact that IT06 estimated it roughly by visually inspecting the oscillations, whereas here, the periods are obtained using wavelet analysis and can be expected to be more reliable. Also, since the helical structure of the filament thread is clearly visible in the images, we consider the filament to be a twisted flux ropelike structure and use the model of Vršnak (1990) to estimate the Alfvén speed. This has led to a different value of Alfvén speed than the one mentioned in IT06.

4. CONCLUSIONS

In this paper, we carried out a detailed wavelet analysis of the large-amplitude oscillation of the polar crown filament. The oscillation was most prevalent around the middle of the filament, with no significant motions detected at the two endpoints. Contrary to IT06, the average period of oscillation is found to be about 2.5–2.6 hr (see Figs. 8 and 9). The oscillation was repeated at least three times before the filament erupted. The period inferred from the wavelet analysis is found to be almost constant along the loop (see Fig. 7), and the *global* oscillation seems to be a standing wave.

The Hα images suggest line-of-sight velocity of few tens of km s^{-1}. In contrast to the previously observed large-amplitude oscillations of the filaments, this one was not excited by a flare or a flarelike event. Magnetic reconnection between a nearby emerging flux and a filament barb is more likely to have triggered the onset of oscillation. We estimated the poloidal and axial components of the magnetic field to be between 2 and 10 G, and 1–5 G, respectively, assuming a twisted flux rope configuration for the filament. These are considered reasonable due to the polar location of the filament.

Prominence seismology is a powerful diagnostic tool for probing various physical parameters of the filament. More observations of similar events and advancements in three-dimensional simulations of flux rope models, in particular a better understanding of MHD waves that such structures support, would lead to a deeper insight into the stability and eruptive aspects of the filaments.

Wavelet software was provided by C. Torrence and G. Compo, and is available at http://atoc.colorado.edu/research/wavelets/. R. J. acknowledges the Nuffield Foundation for an NUF-NAL 04 award. B. P. and D. T. acknowledge the support from STFC.

REFERENCES

Ballai, I. 2003, A&A, 410, L17
Ballester, J. L. 2006, Philos. Trans. R. Soc. London A, 364, 405
Bruzek, A. 1952, Z. Astrophys., 31, 99
Chen, P. F., & Shibata, K. 2000, ApJ, 545, 524
Chifor, H., Mason, H. E., Tripathi, D., Isobe, H., & Asai, A. 2006, A&A, 458, 965
Delaboudiniere, J.-P., et al. 1995, Sol. Phys., 162, 291
Díaz, A. J., Oliver, R., & Ballester, J. L. 2001, A&A, 379, 1083
Domingo, V., Fleck, B., & Poland, A. I. 1995, Sol. Phys., 162, 1
Eto, S., et al. 2002, PASJ, 54, 481
Feynman, J., & Martin, S. F. 1995, J. Geophys. Res., 100, 3355
Isobe, H., & Tripathi, D. 2006, A&A, 449, L17 (IT06)
Isobe, H., Tripathi, D., Asai, A., & Jain, R. 2007, Sol. Phys., 246, 89
Jing, J., Lee, J., Spirock, T. J., & Wang, H. 2006, Sol. Phys., 236, 97
Jing, J., et al. 2003, ApJ, 584, L103
Kippenhahn, R., & Schlüter, A. 1957, Z. Astrophys., 43, 36
Kleczek, J., & Kuperus, M. 1969, Sol. Phys., 6, 72
Lin, J., Forbes, T. G., & Isenberg, P. A. 2001, J. Geophys. Res., 106, 25053
Moreton, G. E. 1960, AJ, 65, 494
Okamoto, T. J., Nakai, H., & Keiyama, A. 2004, ApJ, 608, 1124
Oliver, R., & Ballester, J. L. 2002, Sol. Phys., 206, 45
Oliver, R., Ballester, J. L., Hood, A. W., & Priest, E. R. 1992, ApJ, 400, 369
Ramsey, H. E., & Smith, S. F. 1966, AJ, 71, 197
Roberts, B. 2000, Sol. Phys., 193, 139
Ruderman, M., & Roberts, B. 2002, ApJ, 577, 475
Terradas, J., Corbonell, M., Oliver, R., & Ballester, J. L. 2005, A&A, 434, 741
Thompson, B. J., et al. 1999, ApJ, 517, L151
Tripathi, D. 2005, Ph.D. thesis, Univ. Goettingen
Tripathi, D., Isobe, H., & Mason, H. E. 2006a, A&A, 453, 1111
Tripathi, D., Zanna, D. G., Mason, H. E., & Chifor, C. 2006b, A&A, 460, L53
Vršnak, B. 1990, Sol. Phys., 129, 295
———. 1993, Hvar Obs. Bull., 17, 23
Vršnak, B., Ruždjak, V., & Rompolt, B. 1991, Sol. Phys., 136, 151
Vršnak, B., Veronig, A. M., Thalmann, J. K., & Zic, T. 2007, A&A, 471, 295
Wang, Y. M., & Sheeley, N. R., Jr. 1999, ApJ, 510, L157